ACADEMIA ROMÂNĂ
Revue Roumaine de Chimie
https://www.icf.ro/rrch/

Rev. Roum. Chim.,
2024, *69*(5–6), 285–290
DOI: 10.33224/rrch.2024.69.5-6.06

Dedicated to Professor Vasile Pârvulescu on the occasion of his 70th anniversary

CQDs-BASED NANOCOMPOSITES FOR THE 5-(HYDROXYMETHYL)FURFURAL PHOTOOXIDATION

Giuseppe STOIAN, Elena E. TOMA, Petruța OANCEA, Natalia CANDU, Bogdan COJOCARU, Mădălina TUDORACHE and Simona M. COMAN*

Faculty of Chemistry, University of Bucharest, Regina Elisabeta Blvd., no. 4–12, Bucharest 030016, Roumania

Received February 12, 2024

Carbon quantum dots (CQDs) are widely investigated as an enhancing photocatalytic component of various nanocomposites. With this aim hetero-structures containing CQDs associated to metal oxides were prepared following a hydrothermal approach in which commercial ZnO and TiO_2 P-25 Degussa were used as carriers. CQDs were synthesized in advance by a low-temperature hydrothermal (LHT) treatment of useless humins wastes produced by the glucose dehydration in an acidic medium. Their photocatalytic behavior was investigated in the HMF selective oxidation. The obtained results revealed electronic interactions between CQDs and MOx (*i.e.*, ZnO and TiO_2) which have as effect the enhancement of the charge separation and diminution of the charge recombination. The influence of CQDs and buffer addition on the products distribution was evaluated. The highest photocatalytic efficiency corresponded to the TiO_2/$CQD_{180\text{-}12}$ heterostructure: under UV irradiation FDCA was produced in 360 min with a selectivity of 35.5% for a conversion of 93.4% of HMF.

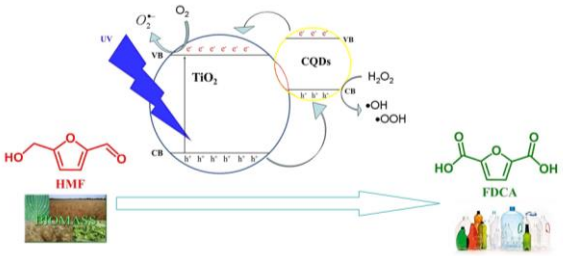

INTRODUCTION

The integration of photocatalysis with biomass utilization emerges as a novel and promising approach to achieve a higher level of sustainability in chemical processes.[1] In this context, the selective oxidation of 5-hydroxymethylfurfural (HMF) to various valuable chemicals, such as 2,5-diformylfuran (DFF), 5-hydroxymethylfuran-2-carboxylic acid (HMFCA), 5-formyl-2-carboxylic acid (FFCA), and 2,5-furandicarboxylic acid (FDCA) (Scheme 1), has garnered significant attention in the field of catalytic and photocatalytic reactions for biomass valorization due to its practical significance.[2–4]

However, the development of effective photocatalysts capable of generating oxidative species which possess the appropriate oxidation power to convert HMF into furanic compounds rather than over-oxidizing it to CO_2 and H_2O remains an important and unfulfilled objective.[5]

Among different UV-active materials titanium dioxide (TiO_2) is the benchmark photocatalyst but ZnO has also received significant attention in this field.[6,7] Due to the closed bandgap energy and the similar reaction mechanism on the two materials it

* Corresponding author: simona.coman@chimie.unibuc.ro

is hypothetically assumed that they have the same photocatalytic ability. With another words ZnO should be a suitable alternative of TiO_2 in photocatalysis. However, a major drawback in photocatalytic efficiency of both materials resides in their ineffective utilization of visible light and a fast recombination of photogenerated electron-hole pairs.[8,9]

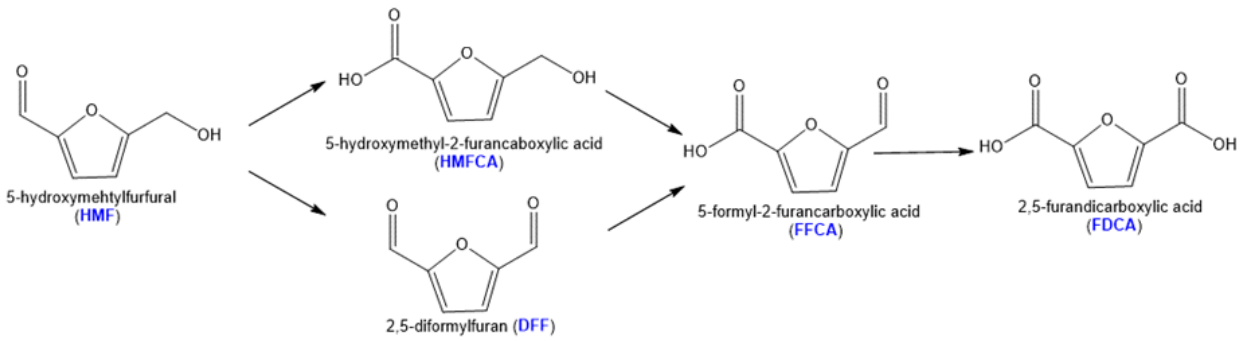

Scheme 1 – Reaction pathways for 5-hydroxymethylfurfural (HMF) oxidation.

Consequently, extensive research has been conducted to enhance their efficiency by modifying their surface-bulk structure and altering the charge transfer pathways to inhibit surface-bulk charge carrier recombination.[9] In this context, recent studies have demonstrated that carbon quantum dots (CQDs) offer potential advantages in addressing the limitations of both TiO_2 and ZnO.[10,11] CQDs play a crucial role in facilitating charge separation, promoting the generation of reactive oxygenated free radicals, enhancing optical absorption in the visible light range, and improving the adsorption capacity for various emergent pollutants.[12,13]

Based on this state of the art, the main objective of the present study was to design an effective photocatalytic system able to selectively oxidize HMF. In accordance, we turned our attention to the recently developed ZnO/CQD nanocomposites in our group.[13] Additionally, TiO_2/CQD nanocomposites were synthesized, characterized and tested in the HMF photooxidation.

RESULTS AND DISCUSSION

The synthesis and characterization of ZnO/CQDs nanocomposites are described and discussed in detail in Ref. [13] and their main characteristics are given in Table 1. The quantum yield (QY) (λ_{ex} = 366 nm) values of the CQDs vary as follows: $CQD_{200\text{-}4}$ (22.6%) > $CQD_{180\text{-}12}$ (21%) > $CQD_{180\text{-}4}$ (8%). The higher QY of $CQD_{200\text{-}4}$ is attributed to its slightly smaller concentration of non-radiative recombination carboxyl (–COOH) sites while the increased QY value of the $CQD_{180\text{-}12}$ can be justified by their smaller size compared to $CQD_{180\text{-}4}$.[13] Under UV irradiation the CQDs function as electron reservoirs, impeding the recombination of electron-hole pairs. This essential feature induced to ZnO/CQDs nanocomposites the high ability to degrade methylene blue (MB) under UV irradiation at a conversion of 99.3% in only 30 min and over 97.6% under visible light irradiation, in 180 min.[13]

The similar XRD patterns of the TiO_2 carrier and TiO_2/CQD nanocomposite demonstrate that the structure of carrier was not modified by the CQDs presence these being just well deposited and with a high dispersion on the TiO_2 surface without any incorporation in its lattice.[14] The electronic interaction between MO_x carrier (where M = Zn, Ti) and CQDs was confirmed by the DRIFT spectroscopy. Therefore, the presence of a novel absorption band, at 1338–1355 cm^{-1}, in the DRIFT spectra of the MO_x/CQD nanocomposite suggest the presence of –COOM– structures that originated from the esterification of the carboxyl groups from CQDs with the hydroxyls groups from MO_x (Scheme 2).[15]

The photo-response of MO_x and MO_x/CQD nanocomposite was measured by DR-UV-Vis spectroscopy. The reflectance spectra were transformed to the corresponding absorption spectra by applying the Kubelka Munk function,[16] and the band gaps (E_g) were estimated from the x-intercept of linear portion of Tauc's plot $((\alpha h\nu)^{1/2}$ versus $h\nu$, at α = 0.[17] The studied samples are shown in Table 1.

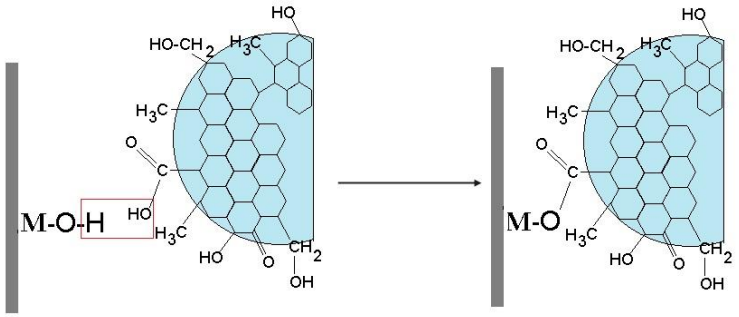

Scheme 2 – Schematically representation of the esterification reaction between the carboxyl groups from CQDs and the hydroxyls groups from MO_x (where M = Zn, Ti).

Table 1

The main characterization data obtained from XRD, DR-UV-Vis spectroscopy and BET measurements

Entry	Sample	Crystallite size, nm[a]	λ, nm	E_g ±0.03, eV[b]	S_{BET}, m^2/g	Ref.
1	ZnO(C)	33.6	368	3.37	12	[13]
2	$ZnO/CQD_{200\text{-}4}$	35.4	414	2.99	15	[13]
3	$ZnO/CQD_{180\text{-}12}$	35.1	404	3.05	18	[13]
4	TiO_2 P-25	20.0	384	3.23	54	This work
5	$TiO_2/CQD_{200\text{-}4}$	19.8	408	3.04	53	This work
6	$TiO_2/CQD_{180\text{-}12}$	19.9	411	3.01	46	This work

[a] – calculated with the Debye-Scherrer equation; [b]– obtained from Tauc plots

Estimated crystalline sizes from XRD analysis indicate the presence of smaller oxide particles in the TiO_2 – based materials. Moreover, BET measurements demonstrated that TiO_2 – based materials has larger surface area. The deposition of CQDs lead to a shift in absorption in the visible range of both ZnO and TiO_2/CQDs nanomaterials.

The prepared materials were tested in the photocatalytic oxidation of HMF in water and UV radiation (fluorescent black lamps (Philips, 8W) that emit at 365 nm). In order to prevent any changes in the pH of the reaction solution and to enhance the selectivity towards oxygenated HMF compounds by avoiding excessive and non-selective over-oxidation, part of the photocatalytic tests were performed in the presence of a $Na_2CO_3/NaHCO_3$ buffer solution (pH = 9.2). It is worth mentioning that Na_2CO_3 base has been previously reported to act as a scavenger for •OH radicals.[18] A comparison of the obtained results in terms of HMF conversion on the $ZnO/CQD_{180\text{-}12}$ catalyst, with and without $Na_2CO_3/NaHCO_3$ buffer (pH = 9.2) and on the ZnO/CQDs nanocomposites in comparison with the pristine ZnO (C) are presented in Figs. 1 and 2.

As Fig. 1 shows, in the absence of the buffer, the conversion of HMF is slightly lower (1.4–21.6%) during the initial 6h of the reaction and the only oxidation product that could be identified was DFF, with selectivities varying in the range of 60.3–100% (Fig. 3). With longer reaction times, HMF was completely converted but it is important to note that this conversion is primarily a result of the HMF over-oxidation. Therefore, after 12h, no organic compounds were detected in the liquid phase (Fig. 3). Most probably, when highly oxidizing species are formed in the photocatalytic system non-selective processes become dominant leading to over-oxidation (*i.e*, CO_2 and H_2O) and thereby resulting in low or even absent oxidation products. After the addition of the buffer, a notable outcome is the slight enhancement in HMF conversion (10–28.6%) during the initial 6h of the reaction (Fig. 1). Furthermore, it appears that the total oxidation of organic compounds is also prevented (Fig. 4), HMFCA, with selectivities of 0.3–18.7%, and lactic acid, with 81.3–99.7% selectivity, being identified in the reaction products (Fig. 4). However, the selectivity to HMFCA predominates at the beginning of the reaction when the conversions of HMF are low. When increasing the HMF conversion, a significant enhancement of lactic acid was observed, suggesting the presence of the CQDs also cause degradation reactions (Fig. 4).

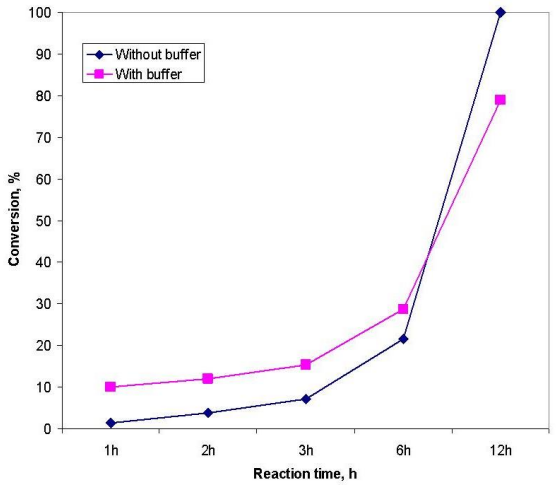

Fig. 1 – The variation of the HMF conversion in time, in the presence of the ZnO/CQD$_{180\text{-}12}$ catalyst.

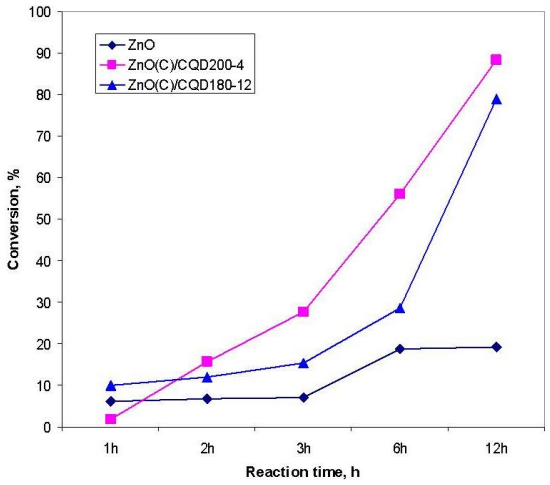

Fig. 2 – The variation of the HMF conversion in time, in the presence of the ZnO(C), ZnO/CQD$_{180\text{-}12}$ and ZnO/CQD$_{200\text{-}4}$ catalysts.

The two different pathways of HMF oxidation in the presence and in the absence of the buffer are in agreement with the findings of Yurdakal *et al*.[5] which also reported that in the absence of a base, HMF is mainly converted to DFF, which can either be transformed into FFCA or goes through a ring-opening reaction to aliphatic products and CO_2 while, in the presence of a base, the oxidation reaction pathway is mainly towards HMFCA.

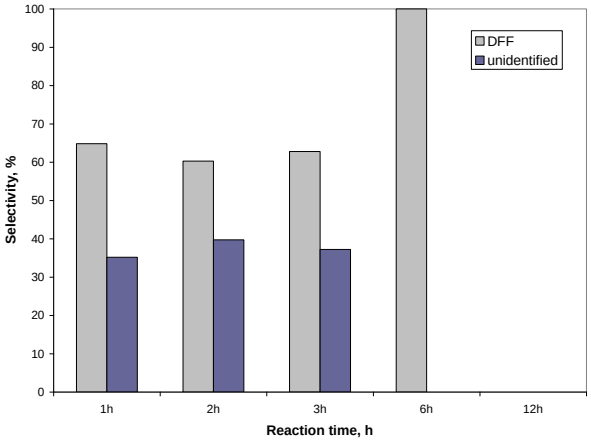

Fig. 3 – The variation of the selectivities to DFF and degradation by-products as a function of time, in the presence of ZnO/CQD$_{180\text{-}12}$ catalyst and in the absence of the buffer.

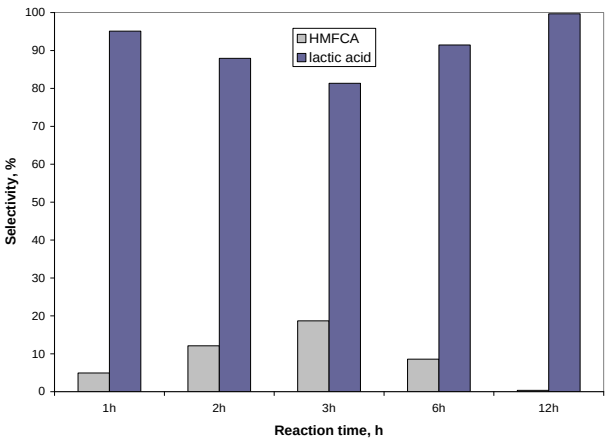

Fig. 4 – The variation of the selectivities to HMFCA and lactic acid (LA) in the presence of ZnO/CQD$_{180\text{-}12}$ catalyst and Na_2CO_3/$NaHCO_3$ buffer (pH = 9.2).

The improvement of the photocatalytic activity of ZnO after its interaction with CQDs can be attributed to the efficient charge separation caused by the rapid photo-induced charge transfer and the inhibition of the electron–hole pairs recombination.[19] The photocatalytic activity was higher in the presence of ZnO/CQD$_{200\text{-}4}$ than in the presence of the ZnO/CQD$_{180\text{-}12}$ while the HMFCA was formed in the presence of all photocatalytic systems, irrespective of the CQDs nature (Fig. 2).

TiO_2/CQDs samples display a different photocatalytic behavior by comparing with the ZnO/CQDs catalytic systems. In the absence of the buffer, only low selectivities to DFF (< 10%) for HMF conversions of less than 5.0% were obtained, irrespective of the CQDs nature. However, in the presence of the buffer and the TiO_2/CQD$_{200\text{-}4}$ nanocomposite, FFCA was generated with a selectivity of 10.4% for a conversion of HMF of 78.8% after 6h, while on TiO_2/CQD$_{180\text{-}12}$ catalyst a selectivity of 6.7% in FDCA for a conversion of HMF of 29.5% was obtained after a similar reaction time. An effective improvement of the photocatalytic efficiency was observed with the

addition of H_2O_2 (46μL) to the system alongside with the buffer. In this system, a selectivity to FDCA of 24.0% was obtained for a conversion of 80.0% of HMF in the presence of $TiO_2/CQD_{200\text{-}4}$, while $TiO_2/CQD_{180\text{-}12}$ lead to FDCA with a selectivity of 35.5% for a conversion of 93.4% of HMF. These results suggest that reactive oxygen intermediates, together with H_2O_2 are responsible for the selective photocatalytic oxidation of HMF. The obtained results are superior to those obtained by Palmisano et al [13] which reported that the highest selectivity to DFF achieved by titania until now is only 22% at 50% HMF conversion in an aqueous medium under UV light (λ = 365 nm) irradiation.

EXPERIMENTAL

The synthesis of carbon quantum dots (CQDs): The CQDs were produced by applying a low temperature hydrothermal (LTH) methodology in which the humins, generated from the decomposition of glucose in acidic medium, were used as raw material. LTH approach was applied at 200 °C for 4h ($CQD_{200\text{-}4}$) and 180 °C for 12 h ($CQD_{180\text{-}12}$).

The synthesis of ZnO/CQDs and TiO_2/CQDs nanocomposites: The ZnO/CQDs nanocomposites were produced by applying a previously procedure reported in literature by using an hydrothermal approach.[13] The hydrothermal approach consists in adding the commercial ZnO (denoted ZnO(C)) in an aqueous solution of CQDs. The slurry was stirred at room temperature for 4 hours and at 140°C for 4 h. After hydrothermal treatment, the solid product was collected by centrifugation, washed with deionized water several times and dried in air for 12 h at 80°C. The same hydrothermal method was used for the synthesis of TiO_2/CQDs nanocomposites. As carrier for CQDs deposition a commercial TiO_2 P-25 Degussa powder (consisting of ca. 85% anatase and 15% rutile in the crystalline phase) was used. Obtained samples were denoted $ZnO/CQD_{200\text{-}4}$, $ZnO/CQD_{180\text{-}12}$, $TiO_2/CQD_{200\text{-}4}$ and $TiO_2/CQD_{180\text{-}12}$.

Nanocomposites characterization: Photoluminescence (PL) spectra of CQDs were measured with a JASCO FP-8200 fluorescence spectrometer equipped with of 150 W xenon lamp as the excitation source, while CQDs-based nanocomposites were characterized by techniques as: adsorption-desorption isotherms of liquid nitrogen at 77K, X-ray diffraction (XRD), IR diffuse reflectance with Fourier transform (DRIFT) spectroscopy and UV-Vis spectroscopy. Experimental measurements details are given in Ref. [13].

Photocatalytic oxidation of HMF: Photocatalytic oxidation of HMF was performed in a cylindrical quartz photoreactor irradiated by fluorescent black lamps (Philips, 8W) that emit at 365 nm. In a typical experiment, 20 mg of catalyst were added to 10 mL of 0.5 mM HMF aqueous solution. The reaction temperature was rigorously maintained at 30 °C using a water-cooling system. The photocatalytic experiments were carried out at a constant pH of 9.2 maintained by a $Na_2CO_3/NaHCO_3$ buffer. The suspension of the photocatalyst and the homogeneity of the reacting mixture were ensured by magnetic stirring. Before switching on the lamp, the suspension was kept in darkness for 15 min and under stirring to reach the thermodynamic equilibrium. Before and during the run, the aqueous suspension was in contact with atmospheric air so that it has been assumed that the dissolved oxygen concentration was always in equilibrium with that of the atmosphere. The HMF amounts adsorbed by the catalysts under dark conditions were always quite low, *i.e.*, less than 2% of the starting HMF amount.

The analysis of the HMF photooxidation products: During one reaction run, samples of reacting suspension (450 μL) were withdrawn at 1, 2, 3, 6, 12, and 24 h, filtered through a 0.45 μm hydrophilic membrane (HA, Millipore) and mixed with 450 μL of H_2SO_4 0.01N before being analyzed. The quantitative determination and identification of the species present in the liquid was performed by means of a HPLC modular system (Agilent Technology 1260 Infinity with DAD and RID detectors) equipped with Zorbax SAX column (4.6 × 250 mm, 5 micron). The experimental conditions of HPLC analysis consist in 0.01N H_2SO_4 as mobile phase with 0.05 $cm^3 \cdot min^{-1}$ flow rate, 10 μL injection volume, 45 °C detector temperature and 30 min analysis time. Identification of the sample components were performed based on the retention time of the corresponding standards (Sigma Aldrich). Because each compound exhibits a different light absorption profile with maxima at 262, 258, 281, 283, and 288 nm for FDCA, HMFCA, FFCA, HMF, and DFF, respectively, detection wavelengths of 254, 262 and 285 nm were chosen for their identification.

CONCLUSIONS

Presented results merely give an overview of the reaction mechanism for HMF photooxidation, which is influenced by the photocatalyst nature, the presence of the CQDs sensitizers and the presence of the buffer (pH = 9.2). The results obtained on ZnO/CQDs materials suggest that these materials are not suitable photocatalysts for the selective oxidation of HMF. It seems the CQD only improves the accessibility of the reactant but do not disables the hydroxyl radical generation by ZnO, responsible for the mineralization. On $ZnO/CQD_{180\text{-}12}$ catalyst and in the absence of the buffer, DFF could be obtained with selectivities varying in the range of 60.3–100% for low HMF conversions (1.4–21.6%). The presence of the buffer led to a change in the reaction mechanism, the HMF photooxidation leading to low selectivities to HMFCA. Contrarily, materials based on TiO_2 were shown to be active and selective in the HMF photooxidation, forming FFCA and FDCA as the most important products.

Therefore, TiO_2/$CQD_{180\text{-}12}$ lead to FDCA with a selectivity of 35.5% for a conversion of 93.4% of HMF, in the presence of the buffer and H_2O_2 as oxidant and to the best of our knowledge, this work represents the system with highest FDCA generation efficiency among all reported CQD-sensitized materials. Nevertheless, in order to find which radicals are involved in oxidation products formation using the presented photocatalytic materials, some additional tests are currently ongoing.

REFERENCES

1. X. Yang and D. Wang, *ACS Appl. Energy Mater.*, **2018**, *1*, 6657–6693.
2. C. M. Pichler, M. G. A. Shaal, H. Joshi, W. Ciptonugroho and F. Schüth, *Chem. Sus. Chem.*, **2018**, *11*, 2083–2090.
3. H. Zhang, Q. Wu, C. Guo, Y. Wu and T. Wu, *ACS Sustain. Chem. Eng*., **2017**, *5*, 3517–3523.
4. Y. Zhou, J. Liu and J. Long, *J. Solid State Chem.*, **2021**, *303*, 122510.
5. S. Yurdakal, B.S. Tek, O. Alagöz, V. Augugliaro, V. Loddo, G. Palmisano and L. Palmisano, *ACS Sustain. Chem. Eng.*, **2013**, *1*, 456–461.
6. X. B. Chen and S. S. Mao, *Chem. Rev*., **2007**, *107*, 2891–2959.
7. A. B. Djurišić, X. Chen, Y. H. Leung and A. Man Ching Ng, *J. Mater. Chem.*, **2012**, *22*, 6526–6535.
8. X. Li, J. Yu and M. Jaroniec, *Chem. Soc. Rev.*, **2016**, *45*, 2603–2636.
9. S. G. Kumar and K. S. R. K. Rao, *RSC Adv.*, **2015**, *5*, 3306–3351.
10. J. Tian, Y. Leng, Z. Zhao, Y. Xia, Y. Sang, P. Hao, J. Zhan, M. Li and H. Liu, *Nano Energy*, **2015**, *11*, 419–427.
11. S. Muthulingam, I. H. Lee and P. Uthirakumar, *J. Colloid Interface Sci.*, **2015**, *455*, 101–109.
12. M. Shalahuddin Al Ja'farawy, Kusumandari; A. Purwanto and H. Widiyandari, *Environ. Nanotech. Monit. Manag.* **2022**, *18*, 100681
13. E. E. Toma, G. Stoian, B. Cojocaru, V. I. Parvulescu and S. M. Coman, *Catalysts*, **2022**, *12*, 952–970.
14. X. J. Lu, W. G. Yang, Z. W. Quan, T. Q. Lin, L. G. Bai, L. Wang, F. Q. Huang and Y. S. Zhao, *J. Am. Chem. Soc.*, **2014**, *136*, 419–426.
15. B.Y. Yu and S.Y. Kwak, *J. Mater. Chem*., **2012**, *22*, 8345–8353.
16. P. Kubelka, *J. Opt. Soc. Am.*, **1948**, *28*, 448–457.
17. J. C. Yu, J. G. Yu, W. K. Ho, Z. T. Jiang and L. Z. Zhang, *Chem. Mater.*, **2002**, *14*, 3808–3816.
18. B. Zhou, J. Song, Z. Zhang, Z. Jiang, P. Zhang and B. Han, *Green Chem*., **2017**, *19*, 1075–1081.
19. J. Xie, Y. Li, W. Zhao, L. Bian and Y. Wei, *Powder Technol.*, **2011**, *207*, 140–144.